Available online at www.sciencedirect.com
ScienceDirect
Journal of Solid State Chemistry 180 (2007) 523–532
JOURNAL OF SOLID STATE CHEMISTRY
www.elsevier.com/locate/jssc

Thermodynamic studies on $SrFe_{12}O_{19}$(s), $SrFe_2O_4$(s), $Sr_2Fe_2O_5$(s) and $Sr_3Fe_2O_6$(s)

S.K. Rakshit*, S.C. Parida, S. Dash, Z. Singh, B.K. Sen, V. Venugopal

Product Development Section, RC & I Group, Bhabha Atomic Research Centre, Trombay, Mumbai-400085, India

Received 20 September 2006; received in revised form 8 November 2006; accepted 8 November 2006
Available online 16 November 2006

Abstract

The citrate–nitrate gel combustion route was used to prepare $SrFe_2O_4$(s), $Sr_2Fe_2O_5$(s) and $Sr_3Fe_2O_6$(s) powders and the compounds were characterized by X-ray diffraction analysis. Different solid-state electrochemical cells were used for the measurement of emf as a function of temperature from 970 to 1151 K. The standard molar Gibbs energies of formation of these ternary oxides were calculated as a function of temperature from the emf data and are represented as

$\Delta_f G_m^\circ$ ($SrFe_2O_4$, s, T)/kJ mol^{-1} (± 1.7) $= -1494.8 + 0.3754\,(T/\mathrm{K})$ ($970 \leqslant T/\mathrm{K} \leqslant 1151$).

$\Delta_f G_m^\circ$ ($Sr_2Fe_2O_5$, s, T)/kJ mol^{-1} (± 3.0) $= -2119.3 + 0.4461\,(T/\mathrm{K})$ ($970 \leqslant T/\mathrm{K} \leqslant 1149$).

$\Delta_f G_m^\circ$ ($Sr_3Fe_2O_6$, s, T)/kJ mol^{-1} (± 7.3) $= -2719.8 + 0.4974\,(T/\mathrm{K})$ ($969 \leqslant T/\mathrm{K} \leqslant 1150$).

Standard molar heat capacities of these ternary oxides were determined from 310 to 820 K using a heat flux type differential scanning calorimeter (DSC). Based on second law analysis and using the thermodynamic database FactSage software, thermodynamic functions such as $\Delta_f H^\circ(298.15\,\mathrm{K})$, $S^\circ(298.15\,\mathrm{K})$ $S^\circ(T)$, $C_p{}^\circ(T)$, $H^\circ(T)$, $\{H^\circ(T)–H^\circ(298.15\,\mathrm{K})\}$, $G^\circ(T)$, free energy function (*fef*), $\Delta_f H^\circ(T)$ and $\Delta_f G^\circ(T)$ for these ternary oxides were also calculated from 298 to 1000 K.

Keywords: Magnetic materials; Strontium hexaferrite; Solid-state galvanic cell; Differential scanning calorimetry (DSC); Curie temperature; Thermodynamic properties

1. Introduction

$SrFe_{12}O_{19}$(s), $SrFe_2O_4$(s), $Sr_2Fe_2O_5$(s) and $Sr_3Fe_2O_6$(s) are few stoichiometric ternary oxides exist in $SrO–Fe_2O_3$ binary system and stable in air [1,2]. In particular, strontium hexaferrite ($SrFe_{12}O_{19}$) crystallizes in the magnetoplumbite hexaferrite structure (*M*-phase) and is widely used as hard ceramic permanent magnetic material and used in high-density recording media, microwave devices and DC motors for the automotive industry and consumer goods [3]. This ferrite crystallizes in a hexagonal structure with 64 ions per unit cell on 11 different symmetry sites ($P6_3/mmc$ space group). The 24 Fe^{3+} atoms are distributed over five distinct sites: three octahedral sites, one tetrahedral site, and one bi-pyramidal site. The magnetic structure is ferrimagnet with five different sublattices: three parallel and two antiparallels [4]. This *M*-type hexaferrite has a very large saturation magnetization, a large uniaxial magnetic anisotropy, and a high curie temperature, which have been widely used as permanent magnetic materials [5]. Strontium hexaferrite powders can exhibit a high coercivity due to the relatively high magneto-crystalline anisotropy field. Several techniques have been used to prepare strontium ferrites such as ball milling [6], salt melting [7], chemical precipitation [8], glass crystallization [9] and self-propagating high temperature synthesis [10]. A chemical route can be excellent method for the synthesis of high pure multi-component oxide due to better homogeneity, better compositional control and lower processing temperatures which are few potential advantages of this wet chemical route over the conventional solid state reaction method [11]. System Sr–Fe–O has been studied extensively with respect to their preparation, characterization, crystallographic, and magnetic properties [1–12], but very few

*Corresponding author. Fax: +91 22 25505151.
E-mail addresses: swarup_kr@rediffmail.com, swarupkr@barc.gov.in (S.K. Rakshit).

0022-4596/$ - see front matter © 2006 Elsevier Inc. All rights reserved.
doi:10.1016/j.jssc.2006.11.012

studies has dealt with its thermodynamic and thermal properties of the ternary compounds of the system [1,13]. Rakshit et al. [13] have already reported the standard molar Gibbs free energy of formation and the molar heat capacities of strontium hexaferrite, $SrFe_{12}O_{19}$(s). Same authors also reported a heat capacity anomaly at 732 K for $SrFe_{12}O_{19}$(s) due to the magnetic order–disorder transition from ferrimagnetic state to paramagnetic state. Many synthesis techniques such as sputtering, organometallic chemical vapor deposition, laser ablation and liquid phase epitaxy (LPE) have been tested for the growth of high quality thin films of strontium hexaferrite. Most of these synthesis processes use low oxygen partial pressures ($<10^{-6}$ kPa) and moderately high temperature. Hence for reproducible synthesis of magnetic thin films with the desired structure and magnetic properties, information on oxygen potential and standard Gibbs energies of formation of the compounds is required.

Compounds $SrFe_{12}O_{19}$(s), $SrFe_2O_4$(s), $Sr_2Fe_2O_5$(s) and $Sr_3Fe_2O_6$(s) lie on the tie line joining SrO and Fe_2O_3 phases in pseudo-binary system of SrO–Fe_2O_3. Hence, it is possible to setup different electrochemical cells based on CaF_2(s) solid electrolyte to determine the Gibbs free energy of formations of these ternary oxides. In this work, stoichiometric ternary oxides, $SrFe_2O_4$(s), $Sr_2Fe_2O_5$(s) and $Sr_3Fe_2O_6$(s) of Sr–Fe–O system were synthesized by citrate–nitrate gel combustion route and characterized by X-ray diffraction (XRD) analysis and thermodynamic studies have been carried out using solid-state electrochemical technique and differential scanning calorimetry.

2. Experimental

2.1. Materials preparation

Different stoichiometric proportions of $Fe(NO_3)_3 \cdot 9H_2O$ (Qualigens Fine Chemicals, mass fraction 0.995) and $SrCO_3$ (LEICO Ind., USA, mass fraction 0.9999) were dissolved in dilute nitric acid to prepare $SrFe_2O_4$(s), $Sr_2Fe_2O_5$(s) and $Sr_3Fe_2O_6$(s). Excess amount of citric acid (E. Merck, India, mass fraction 0.995) was added to the solution to assist complete dissolution. The resultant solutions were heated on a hot plate around 375 K to remove water and oxides of nitrogen. A gel was formed which was further heated at 450 K to dryness. The residues were ground in an agate mortar and pestle and heated at 1273 K in dry air for 100 h with two intermediate grindings. The resultant products were identified as pure phases of $SrFe_2O_4$(s), $Sr_2Fe_2O_5$(s) and $Sr_3Fe_2O_6$(s) by XRD analysis using a STOE powder X-ray diffractometer with Cu$K\alpha$ radiation using JCPDS file no. 48–0156, 33–0677 and 82–0426, respectively. Preparations of powder samples of $SrFe_{12}O_{19}$(s) were described in details by Rakshit et al. [13]. Powder samples of these oxides were used for heat capacity measurements. Phase mixtures of $\{SrFe_2O_4(s) + SrFe_{12}O_{19}(s) + SrF_2(s)\}$, $\{Sr_2Fe_2O_5(s) + SrFe_2O_4(s) + SrF_2(s)\}$ and $\{Sr_3Fe_2O_6(s) + Sr_2Fe_2O_5(s) + SrF_2(s)\}$ were mixed homogeneously using agate mortar and pestle and palletized using a steel die at a pressure of 100 MPa into a 10 mm dia and 3 mm thick pellet and sintered at 1100 K in purified argon gas atmosphere for 24 h and preserved inside a desiccator for emf measurements.

2.2. Solid-state electrochemical cell with CaF_2 as solid electrolyte

A schematic diagram of a fluoride cell used in this study is shown in Fig. 1. Optical grade single crystal CaF_2 pellet of 6 mm diameter and 3 mm thick (supplied by Solon Technologies, Inc., USA) was used as an electrolyte. It is a single compartment cell with provisions for passing argon gas during the experiment and to measure the temperature of the cell near the electrode/electrolyte interface. High purity argon containing 10 ppm O_2(g) gas at 10^5 Pa was allowed to pass through successive traps of oxidized form of BTS catalysts, molecular sieves, silica gels and anhydrous magnesium perchlorate for removal of traces of hydrogen and moisture. The reference electrode, the electrolyte and the measuring electrode stacked one over the other, was kept in the isothermal zone of a Kanthal wire wound resistance furnace. The furnace temperature was controlled within ± 1 K by using a PID controller. The experimental setup and the cell assembly used in this study have been explained in details in an earlier publication [13].

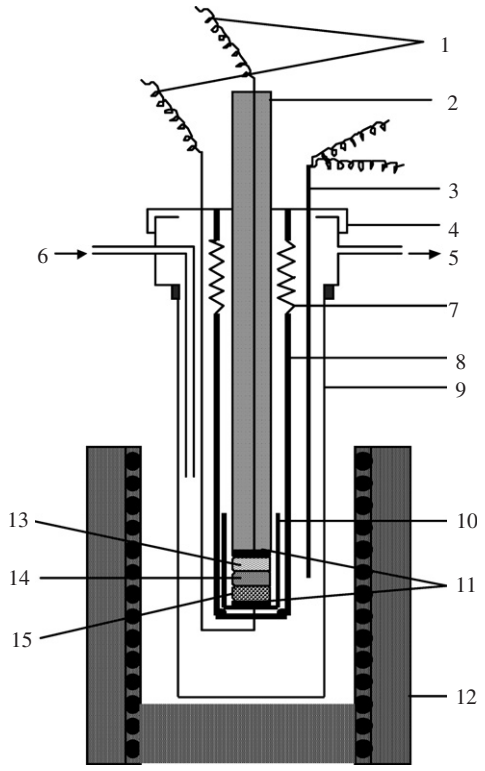

Fig. 1. Schematic diagram of the fluoride cell 1: Pt wires; 2: alumina pressing tube; 3: thermocouple; 4: stainless steel flange; 5: gas inlet; 6: gas outlet; 7: spring; 8: quartz holder; 9: quartz tube; 10: alumina cup; 11: Pt discs; 12: Kanthal wire wound furnace; 13: reference electrode; 14: CaF_2 electrolyte; 15: sample electrode.

Prior to the actual experiments, the experimental cell setup was standardized using two standard electrodes, prepared by phase mixtures of $\{CaO(s)+CaF_2(s)\}$ and $\{MgO(s)+MgF_2(s)\}$ and $CaF_2(s)$ as solid electrolyte. The above cell is represented as

$$\text{Cell (I)}: \ (-)\text{Pt}, \ O_2(g)/\{CaO(s)+CaF_2(s)\}//CaF_2(s)//\{MgO(s)+MgF_2(s)\}/O_2(g), \ \text{Pt}(+).$$

The reversible emfs of the cell was measured as a function of temperature and the Gibbs energy of the net cell reaction was compared with that of literature [14]. After this experiment, the reversible emfs of the following solid-state galvanic cells were measured as a function of temperature.

$$\text{Cell (II)}: \ (-)\text{Pt}, \ O_2(g)/\{CaO(s)+CaF_2(s)\}//CaF_2(s)//\{SrFe_2O_4(s)+SrFe_{12}O_{19}(s)+SrF_2(s)\}/O_2(g), \ \text{Pt}(+).$$

$$\text{Cell (III)}: \ (-)\text{Pt}, \ O_2(g)/\{CaO(s)+CaF_2(s)\}//CaF_2(s)//\{Sr_2Fe_2O_5(s)+SrFe_2O_4(s)+SrF_2(s)\}/O_2(g), \ \text{Pt}(+).$$

$$\text{Cell (IV)}: \ (-)\text{Pt}, \ O_2(g)/\{CaO(s)+CaF_2(s)\}//CaF_2(s)//\{Sr_3Fe_2O_6(s)+Sr_2Fe_2O_5(s)+SrF_2(s)\}/O_2(g), \ \text{Pt}(+).$$

The cell temperature close to the (electrode/electrolyte/electrode) interface was measured using a pre-calibrated (ITS-90) chromel-alumel thermocouple. The cell emf (± 0.2 mV) was measured using a Kiethley 614 electrometer (input impedance $> 10^{14}\,\Omega$). At low temperatures, stable values of emf were obtained nearly after 48 h whereas at successive higher temperatures stability in emf values were observed within 3 to 5 h. The reversibility of the solid-state electrochemical cells was ensured by performing the micro-coulometric titration in both directions. The electrode pellets after the emf experiments were re-examined by XRD analysis and the phase compositions were found unchanged.

2.3. Measurement of molar heat capacity using differential scanning calorimetry

Molar heat capacity measurements were carried out using a heat flux type differential scanning calorimeter (DSC 131, Setaram Instrumentation, France). Temperature calibration for the calorimeter was carried out using the phase transition temperatures of NIST reference materials (indium: $T_{fus} = 429.748$ K; tin: $T_{fus} = 505.078$ K; lead: $T_{fus} = 600.600$ K) and AR grade samples of mercury ($T_{fus} = 234.316$ K), cyclohexane ($T_{fus} = 280.1$ K, $T_{trs} = 190.0$ K), potassium nitrate ($T_{trs} = 400.85$ K) and silver sulfate ($T_{trs} = 703.15$ K). Heat calibration of the calorimeter was carried out using the transition heats of the above-mentioned materials.

To determine the heat capacity as a function of temperature using DSC 131 instrument in continuous heating mode, three sets of experiments were performed. In all experiments, experimental parameters such as initial and end temperature, heating rate, delay time and the carrier gas (argon) flow rate were kept same. In the first experiment, two empty cylindrical flat bottom aluminum crucibles of identical masses of $10^{-4}\,dm^3$ capacity with covering lids were kept inside the furnace over the crucible holders and heat flow as a function of temperature were measured at a heating rate of $5\,K\,min^{-1}$. In the second experiment, heat flow as a function of temperature were measured by taking a known weight (~200 mg) of powdered NIST synthetic sapphire (SRM-720) sample into the aluminum crucible of the sample side keeping the crucible in the reference side empty. In the third experiment, heat flow as a function of temperature were measured by taking a known weight (~200 mg) of preheated powder samples of $SrFe_2O_4(s)$, $Sr_2Fe_2O_5(s)$ and $Sr_3Fe_2O_6(s)$ in the same aluminum crucible one by one and kept in the sample side keeping the crucible in the reference side empty. In order to check the accuracy of the measurement, heat capacity of Fe_2O_3 (mass fraction 0.9999, Alfa Aesar, USA) was measured in the temperature range from 310 to 820 K. The values of heat capacity of $Fe_2O_3(s)$ were found to be within ± 1.5 percent compared to the literature values [14].

3. Results and discussions

3.1. Emf studies on cell (I)–(IV)

3.1.1. Standardization of solid-state galvanic cell (I)

The reversible emf values obtained at different experimental temperatures for cell (I) are listed in Table 1 and the variation of emf with temperature is shown in Fig. 2. The emf data were least squares fitted to yield the following linear relation:

$$E/V\ (\pm 0.0002) = 0.3956 - 2.1038 \times 10^{-5} \times (T/K). \quad (1)$$

The half-cell reactions at each electrode can be represented as

$$MgF_2(s) + 2e^- + 1/2\ O_2(g) = MgO(s) + 2F^- \quad (\text{at} + \text{ve} \quad \text{electrode}) \quad (2)$$

and

$$CaO(s) + 2F^- = CaF_2(s) + 2e^- + 1/2\ O_2(g) \quad (\text{at} - \text{ve} \quad \text{electrode}). \quad (3)$$

Table 1
Variation of emf as a function of temperature for cells (I)–(IV)

Cell (I)		Cell (II)		Cell (III)		Cell (IV)	
T/K	E/V	T/K	E/V	T/K	E/V	T/K	E/V
921	0.3762	970	0.1345	970	0.1013	969	0.0758
960	0.3754	980	0.1330	980	0.1028	976	0.0766
982	0.3749	1000	0.1291	1000	0.1072	998	0.0838
1019	0.3741	1023	0.1243	1015	0.1112	1019	0.0896
1060	0.3733	1043	0.1205	1033	0.1141	1037	0.0950
1101	0.3724	1057	0.1184	1052	0.1172	1058	0.0990
1134	0.3717	1081	0.1158	1073	0.1219	1076	0.1068
1150	0.3714	1098	0.1105	1094	0.1262	1100	0.1141
		1121	0.1064	1115	0.1304	1119	0.1218
		1137	0.1037	1133	0.1340	1136	0.1250
		1151	0.1011	1149	0.1372	1150	0.1292

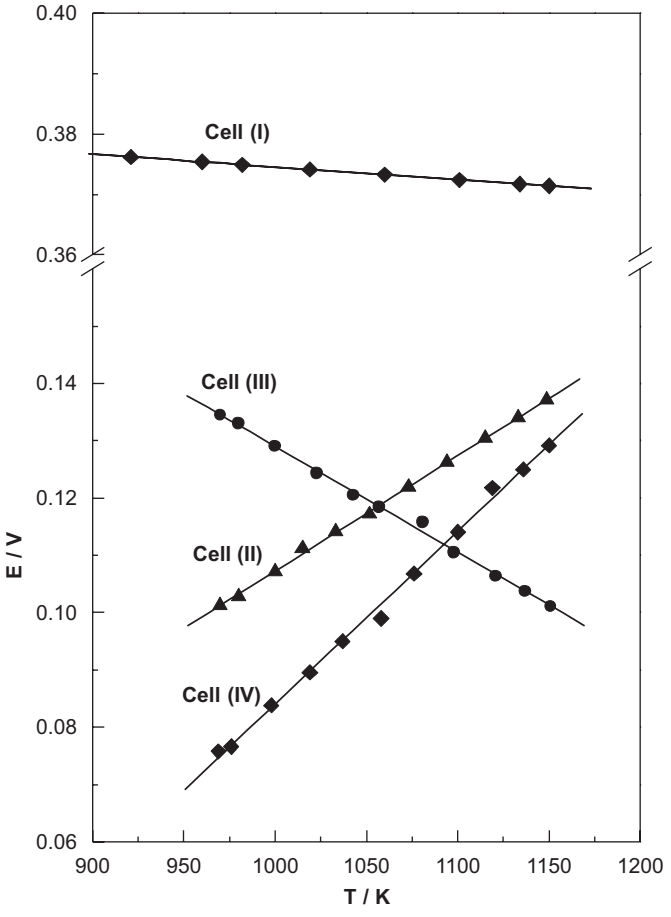

Fig. 2. Variation of emf as a function of temperature for cells (I)–(IV).

The net virtual cell reaction can be represented as

$$MgF_2(s) + CaO(s) = CaF_2(g) + MgO(s) \quad (4)$$

The Gibbs free energy change for the net cell reaction is calculated from the general relation

$$\Delta_r G^\circ = -nFE \quad (5)$$

where, n is the total number of electrons involved in the half cell reactions and F is the Faraday's constant ($F = 96486.4\,C\,mol^{-1}$). The values of $\Delta_r G^\circ(T)$ for reaction (4) as a function of temperature can be calculated using Eqs. (1) and (5) ($n = 2$) and is represented by the following expression:

$$\Delta_r G^\circ(T)/kJ \times mol^{-1}\ (\pm 0.1) = -76.3 + 0.0041 \times (T/K). \quad (6)$$

The values of $\Delta_r G^\circ(T)$ for reaction (4) obtained in this study are in good agreement ($\pm 2.0\,kJ\,mol^{-1}$) with those calculated using the values of standard molar Gibbs free energy of formations for CaF_2(s), MgF_2(s), MgO(s) and CaO(s) from the literature [14].

3.1.2. $\Delta_f G^\circ(T)$ for $SrFe_{12}O_{19}$(s)

Rakshit et al. [13] have already studied this compound and determined its standard molar Gibbs free energy of formation and is represented in Table 2.

According to the reaction:

$$SrO(s) + 6Fe_2O_3(s) = SrFe_{12}O_{19}(s), \quad (7)$$

the standard molar Gibbs energy of formation of $SrFe_{12}O_{19}$(s) from its component oxides SrO(s) and Fe_2O_3(s) in the temperature range from 984 to 1151 K have been calculated from $\Delta_f G^\circ(SrFe_{12}O_{19}, s, T)$ values and the auxiliary data of SrO(s) and Fe_2O_3(s) from the literature [14] and is represented in Table 2.

3.1.3. $\Delta_f G^\circ(T)$ for $SrFe_2O_4$(s)

The reversible emf values obtained at different experimental temperatures for cell (II) are listed in Table 1 and the variation of emf with temperature is shown in Fig. 2. The half-cell reactions at each electrode can be represented as

$$SrFe_{12}O_{19}(s) + 5SrF_2(s) + 10e^- + 5/2\ O_2(g) = 6SrFe_2O_4(s) + 10F^- \quad (at + ve \quad electrode), \quad (8)$$

Table 2
Gibbs energies of formation of ternary compounds of Sr–Fe–O system from its elements ($\Delta_f G_m^\circ$) and its component oxides ($\Delta_{ox} G_m^\circ$)

Compound	Temperature range (K)	$\Delta_f G_m^\circ$/kJ mol^{-1}	$\Delta_{ox} G_m^\circ$/kJ mol^{-1}	Reference
$SrFe_{12}O_{19}$(s)	984–1151	$-5453.5+1.5267\,(T/K)$ (± 1.3)	$-11.6-0.0573\,(T/K)$ (± 0.7)	Rakshit et al. [13]
$SrFe_2O_4$(s)	970–1151	$-1494.8+0.3754\,(T/K)$ (± 1.7)	$-94.3+0.0257\,(T/K)$ (± 1.7)	This study
$Sr_2Fe_2O_5$(s)	970–1149	$-2119.3+0.4461\,(T/K)$ (± 3.0)	$-126.7-0.0056\,(T/K)$ (± 3.0)	This study
$Sr_3Fe_2O_6$(s)	969–1150	$-2719.8+0.4974\,(T/K)$ (± 7.3)	$-135.1-0.0563\,(T/K)$ (± 7.4)	This study

$$5CaO(s) + 10F^- = 5CaF_2(s) + 5/2\ O_2(g) + 10e^- \quad (\text{at } -\text{ve electrode}). \tag{9}$$

Hence, the net cell reaction can be written as

$$SrFe_{12}O_{19}(s) + 5CaO(s) + 5SrF_2(s) = 6SrFe_2O_4(s) + 5CaF_2(s). \tag{10}$$

The emf data were least squares fitted to yield the following linear relation:

$$\text{Cell (II)}: \ E/V\ (\pm 0.0007) = 0.3136 - 1.8456 \times 10^{-4}\,(T/K). \quad (970 \leqslant T/K \leqslant 1151). \tag{11}$$

The Gibbs free energy change for the equilibrium reaction (10) can be calculated using Eq. (5) ($n = 10$) and Eq. (11) and is represented as

$$\Delta_r G^\circ(T)/kJ\,mol^{-1}(\pm 0.7) = -302.6 - 0.1781\,(T/K) \quad (970 \leqslant T/K \leqslant 1151). \tag{12}$$

The standard molar Gibbs energy of formation $\Delta_f G_m^\circ$ ($SrFe_2O_4$, s, T) was obtained by using Eqs. (10) and (12) and values of $\Delta_f G_m^\circ(T)$ for CaF_2(s), SrF_2(s), and CaO(s) from literature [14] and represented in Table 2. According to the reaction

$$SrO(s) + Fe_2O_3(s) = SrFe_2O_4(s), \tag{13}$$

the standard molar Gibbs energy of formation of $SrFe_2O_4$(s) from its component oxides SrO(s) and Fe_2O_3(s) in the temperature range from 970–1151 K have been calculated from $\Delta_f G^\circ$($SrFe_2O_4$, s, T) and the auxiliary data of SrO(s) and Fe_2O_3(s) from the literature [14] and is represented in Table 2.

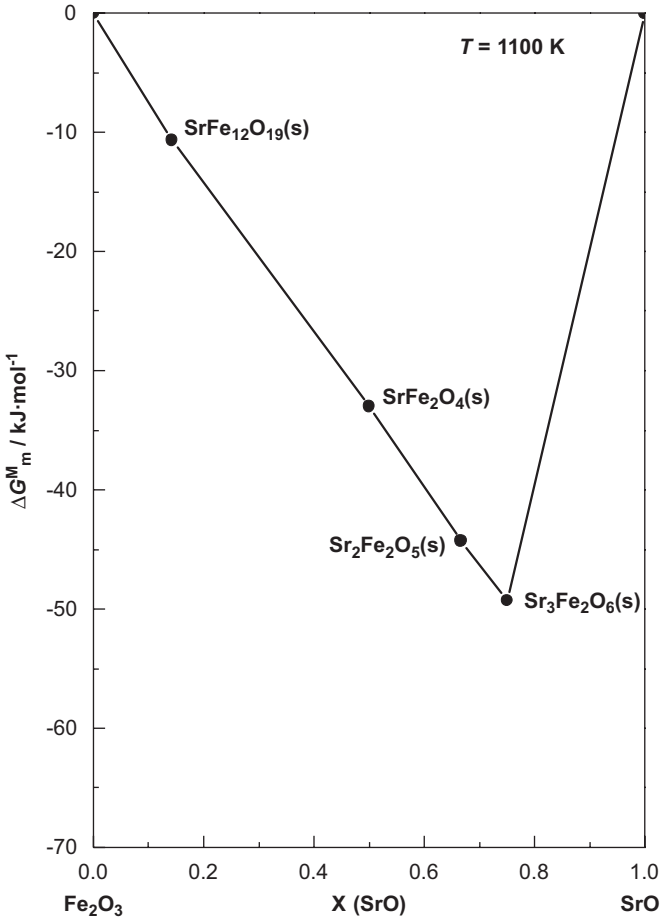

Fig. 3. Gibbs energy of mixing of ternary oxides of the system Sr–Fe–O.

3.1.4. $\Delta_f G^\circ(T)$ for $Sr_2Fe_2O_5$(s)

The reversible emf values obtained at different experimental temperatures for cell (III) are listed in Table 1 and the variation of emf with temperature is shown in Fig. 2. The half-cell reactions at each electrode can be represented as

$$SrFe_2O_4(s) + SrF_2(s) + 2e^- + 1/2\ O_2(g) = Sr_2Fe_2O_5(s) + 2F^- \quad (\text{at} + \text{ve electrode}), \tag{14}$$

$$CaO(s) + 2F^- = CaF_2(s) + 1/2\ O_2(g) + 2e^- \quad (\text{at } -\text{ve electrode}). \tag{15}$$

Hence, the net cell reaction can be written as

$$SrFe_2O_4(s) + CaO(s) + SrF_2(s) = Sr_2Fe_2O_5(s) + CaF_2(s). \tag{16}$$

The emf data were least squares fitted to yield the following linear relation:

$$\text{Cell (III)}: \ E/V\ (\pm 0.0004) = -0.0935 + 2.0081 \times 10^{-4}\,(T/K). \quad (970 \leqslant T/K \leqslant 1149) \tag{17}$$

The Gibbs free energy change for the equilibrium reaction (16) can be calculated using Eq. (5) ($n = 2$) and Eq. (17)

and is represented as

$$\Delta_r G^\circ(T)/\mathrm{kJ\,mol^{-1}}\ (\pm 2.4) = 18.04 - 0.0388\,(T/K) \quad (970 \leqslant T/\mathrm{K} \leqslant 1149). \tag{18}$$

The standard molar Gibbs energy of formation $\Delta_f G_m^\circ$ ($Sr_2Fe_2O_5$, s, T) was obtained by using Eqs. (16) and (18) and values of $\Delta_f G_m^\circ(T)$ for CaF_2(s), SrF_2(s), and CaO(s) from literature [14] and represented in Table 2. According to the reaction:

$$2SrO(s) + Fe_2O_3(s) = Sr_2Fe_2O_5(s), \tag{19}$$

the standard molar Gibbs energy of formation of $Sr_2Fe_2O_5$(s) from its component oxides SrO(s) and Fe_2O_3(s) in the temperature range from 970 to 1149 K was calculated from $\Delta_f G^\circ$($Sr_2Fe_2O_5$, s, T) and the auxiliary data of SrO(s) and Fe_2O_3(s) from the literature [14] and is represented in Table 2.

3.1.5. $\Delta_f G^\circ(T)$ for $Sr_3Fe_2O_6$(s)

The reversible emf values obtained at different experimental temperatures for cell (IV) are listed in Table 1 and the variation of emf with temperature is shown in Fig. 2. The half-cell reactions at each electrode can be represented as

$$Sr_2Fe_2O_5(s) + SrF_2(s) + 2e^- + 1/2\ O_2(g) = Sr_3Fe_2O_6(s) + 2F^-\ (\mathrm{at + ve\ \ electrode}), \tag{20}$$

$$CaO(s) + 2F^- = CaF_2(s) + 1/2\ O_2(g) + 2e^- \quad (\mathrm{at - ve\ \ electrode}). \tag{21}$$

Hence, the net cell reaction can be written as

$$Sr_2Fe_2O_5(s) + CaO(s) + SrF_2(s) = Sr_3Fe_2O_6(s) + CaF_2(s). \tag{22}$$

Table 3
Standard molar heat capacities of $SrFe_{12}O_{19}$(s), $SrFe_2O_4$(s), $Sr_2Fe_2O_5$(s) and $Sr_3Fe_2O_6$(s) as a function of temperature

$C_{p,m}^\circ$/J K^{-1} mol^{-1}					$C_{p,m}^\circ$/J K^{-1} mol^{-1}				
T/K	$SrFe_{12}O_{19}$(s)	$SrFe_2O_4$(s)	$Sr_2Fe_2O_5$(s)	$Sr_3Fe_2O_6$(s)	T/K	$SrFe_{12}O_{19}$(s)	$SrFe_2O_4$(s)	$Sr_2Fe_2O_5$(s)	$Sr_3Fe_2O_6$(s)
310	696.1	148.4	190.5	232.4	492	875.2	170.1	215.5	260.8
319	715.2	149.5	191.8	234.0	500	879.2	171.2	216.7	262.1
328	724.3	150.3	192.8	235.1	509	883.7	172.2	217.9	263.4
338	732.6	151.2	193.9	236.3	518	886.2	173.2	219.0	264.6
348	747.0	152.3	195.1	237.8	527	890.4	174.3	220.1	265.9
357	760.6	153.3	196.3	239.1	536	893.0	175.3	221.3	267.1
367	774.0	154.6	197.8	240.9	544	896.8	176.3	222.4	268.4
375	784.1	155.9	199.3	242.6	552	898.5	177.3	223.5	269.6
385	796.1	157.1	200.8	244.3	560	901.0	178.3	224.6	270.8
395	807.3	158.4	202.2	245.9	569	903.5	179.3	225.7	272.0
404	816.9	159.6	203.6	247.4	578	905.8	180.3	226.8	273.2
414	826.1	160.8	204.9	249.0	586	907.2	181.2	227.9	274.4
422	832.7	161.9	206.3	250.5	591	908.1	181.7	228.4	275.0
432	840.9	163.1	207.6	252.0	600	910.2	182.7	229.5	276.2
442	847.6	164.2	208.9	253.4	610	911.9	183.7	230.6	277.3
450	852.7	165.3	210.1	254.8	619	913.7	184.6	231.6	278.5
459	859.1	166.4	211.4	256.2	628	915.1	185.6	232.7	279.6
468	865.5	167.5	212.6	257.5	637	916.5	186.6	233.7	280.8
478	869.8	168.6	213.8	258.9	647	917.6	187.5	234.8	281.9
657	919.1	188.5	235.8	283.1	736	954.4	195.1	243.1	291.0
662	919.4	189.0	236.4	283.7	740	941.5	195.6	243.6	291.5
666	920.1	189.4	236.9	284.2	745	935.7	196.1	244.1	292.1
670	920.6	189.9	237.4	284.8	750	932.8	196.5	244.6	292.6
674	921.1	190.0	237.5	284.9	754	931.5	197.0	245.1	293.2
679	921.5	190.1	237.6	285.0	758	930.4	197.5	245.6	293.7
684	924.4	190.2	237.7	285.1	762	929.3	197.9	246.1	294.3
688	927.5	190.3	237.8	285.2	767	928.1	198.4	246.7	294.9
692	930.6	190.4	237.9	285.3	772	927.2	198.9	247.2	295.4
696	932.4	190.9	238.4	285.9	777	926.9	199.3	247.7	296.0
700	932.6	191.3	239.0	286.5	782	926.7	199.8	248.2	296.5
705	942.4	191.8	239.5	287.0	786	926.8	200.3	248.7	297.1
710	946.9	192.3	240.0	287.6	795	926.9	201.0	249.5	298.0
714	950.1	192.8	240.5	288.2	803	927.0	202.1	250.5	299.1
718	953.8	193.2	241.0	288.7	811	927.1	203.2	251.6	300.2
722	959.6	193.7	241.5	289.3	815	927.2	203.8	252.3	300.8
727	964.2	194.2	242.1	289.9	820	927.2	204.4	252.9	301.3
732	964.8	194.7	242.6	290.4					

The emf data were least squares fitted to yield the following linear relation:

$$\text{Cell (IV)}: \; E/\text{V}(\pm 0.0011) = -0.2176 + 3.0165 \times 10^{-4}\,(T/\text{K}). \quad (969 \leqslant T/\text{K} \leqslant 1150) \tag{23}$$

The Gibbs free energy change for the equilibrium reaction (22) can be calculated using Eq. (5) ($n = 2$) and Eq. (23) and is represented as:

$$\Delta_r G^\circ(T)/\text{kJ mol}^{-1}(\pm 6.7) = 42.0 - 0.0582\,(T/\text{K}) \quad (969 \leqslant T/\text{K} \leqslant 1150) \tag{24}$$

the standard molar Gibbs energy of formation $\Delta_f G_m^\circ$ ($Sr_3Fe_2O_6$, s, T) was obtained by using Eqs. (22) and (24) and values of $\Delta_f G_m^\circ(T)$ for CaF_2(s), SrF_2(s), and CaO(s) from literature [14] and represented in Table 2. According to the reaction:

$$3\text{SrO(s)} + Fe_2O_3\text{(s)} = Sr_3Fe_2O_6\text{(s)}, \tag{25}$$

the standard molar Gibbs energy of formation of $Sr_3Fe_2O_6$(s) from its component oxides SrO(s) and Fe_2O_3(s) in the temperature range from 969–1150 K was calculated from $\Delta_f G^\circ$($Sr_3Fe_2O_6$, s, T) and the auxiliary data of SrO(s) and Fe_2O_3(s) from the literature [14] and is represented in Table 2.

The Gibbs energies of mixing for ternary oxides of the system SrO–Fe_2O_3 at 1100 K is shown in Fig. 3 as a function of composition of SrO. The values of Gibbs energy of mixing for each ternary oxide are obtained by dividing its standard molar Gibbs energy of formation from the component binary oxides by the number of molecules of the binary oxides present in the compound. It is evident from the figure that $SrFe_{12}O_{19}$(s) is marginally stable relative to its neighbors at 1100 K.

3.2. Measurement of heat capacities of ternary oxides of the system Sr–Fe–O

The isobaric molar heat capacities of $SrFe_2O_4$(s), $Sr_2Fe_2O_5$(s) and $Sr_3Fe_2O_6$(s) as a function of temperature were measured from 310 to 820 K and represented in Table 3. For the sake of completeness, isobaric molar heat capacities of $SrFe_{12}O_{19}$(s) from literature [13] are also shown in Table 3. The variation of heat capacities of these ternary oxides as a function of temperature is shown in Fig. 4. According to Rakshit et al. [13], a heat capacity anomaly was observed for $SrFe_{12}O_{19}$(s) and the transition temperature is found to be 732 K [13]. Berbenni and Marini [1] have also reported the transition temperature for this compound at 713 K. However, it can be seen from their recorded DSC thermogram that the transition temperature is around 733 K, which is in good agreement with our observation. The transition observed in this compound could be assigned to magnetic order–disorder transition

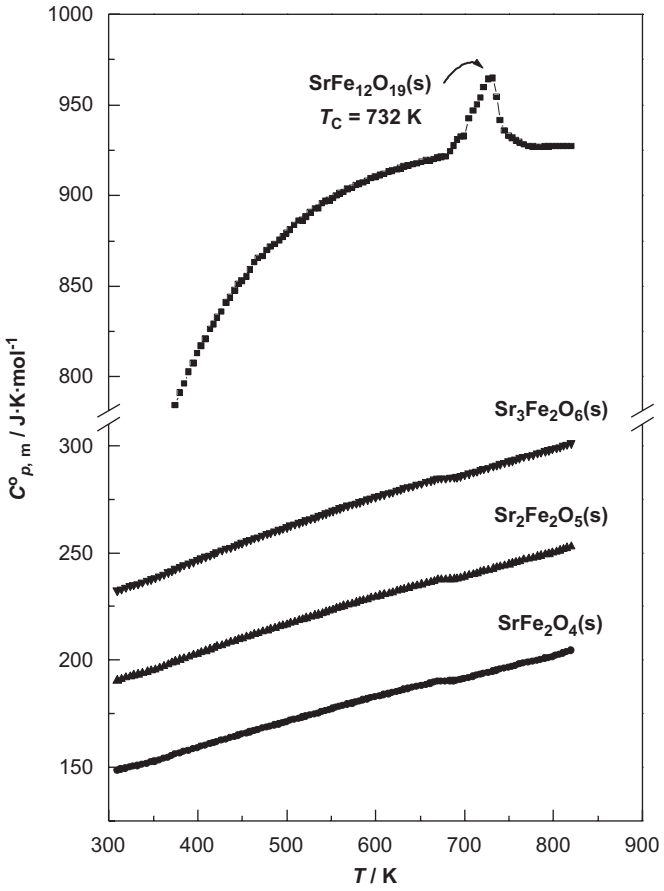

Fig. 4. Variation of standard molar heat capacity of ternary oxides of Sr–Fe–O system as a function of temperature.

Table 4
Molar heat capacities of ternary oxides of Sr–Fe–O system as a function of temperature from 310 to 820 K

Compound	$C_{p,m}^\circ$ (T)/J K^{-1} mol^{-1}	Temperature range (K)	Error (%)
$SrFe_{12}O_{19}$(s)	1038.9–0.0684T–31636035.1/T^2	298–679	2.1
$SrFe_{12}O_{19}$(s)	313.4 + 0.8919T	679–732	2.2
$SrFe_{12}O_{19}$(s)	3097.2–2.9125T	732–740	1.2
$SrFe_{12}O_{19}$(s)	1236.3–0.4024T	740–772	1.5
$SrFe_{12}O_{19}$(s)	922.4 + 0.0058T	772–820	1.4
$SrFe_2O_4$(s)	128.6 + 0.0936T–1037595.7/T^2	298–820	2.0
$Sr_2Fe_2O_5$(s)	172.2 + 0.1005T–1410363.9/T^2	298–820	2.1
$Sr_3Fe_2O_6$(s)	215.4 + 0.1079T–1772263.6/T^2	298–820	2.0

from ferrimagnetic state to paramagnetic state and hence the transition temperature is termed as Curie temperature (T_C). The values of heat capacities of these ternary oxides were best fitted by least squares method as a function of temperature and represented in Table 4. Due to the presence of magnetic transition in $SrFe_{12}O_{19}$(s) at 732 K, heat capacity values were best fitted in different temperature ranges and extrapolated to 1000 K and represented in Table 4.

3.3. Construction of thermodynamic table for ternary oxides of Sr–Fe–O system using second law analysis and FactSage software

Second law analysis and 'FactSage' [15] software were used to construct thermodynamic tables for $SrFe_{12}O_{19}$(s), $SrFe_2O_4$(s), $Sr_2Fe_2O_5$(s) and $Sr_3Fe_2O_6$(s). Thermodynamic table includes the basic functions such as $\Delta_f H^\circ$(298.15 K), S°(298.15 K) $S^\circ(T)$, $C_p{}^\circ(T)$, $H^\circ(T)$, $\{H^\circ(T)–H^\circ(298.15\,K)\}$,

Table 5
Thermodynamic functions for the compound $SrFe_{12}O_{19}$(s)

T/K	$C_p{}^\circ$[a] ($J\,K^{-1}\,mol^{-1}$)	H° ($kJ\,mol^{-1}$)	G° ($kJ\,mol^{-1}$)	S° ($J\,K^{-1}\,mol^{-1}$)	$H^\circ(T)–H^\circ(298.15)$ ($kJ\,mol^{-1}$)	*fef* ($J\,K^{-1}\,mol^{-1}$)	$\Delta_f H^\circ$ ($kJ\,mol^{-1}$)	$\Delta_f G^\circ$ ($kJ\,mol^{-1}$)
Error	1.6%	±1.1	±1.2	±1.1	±0.5	±1.6	±1.2	±1.3
298.15	666.2	−5545.2	−5733.9	633.1	0	633.1	−5545.2	−5038.9
300	670.5	−5543.9	−5735.1	637.2	1.2	637.2	−5545.1	−5035.9
350	762.5	−5507.9	−5769.8	748.0	37.0	747.9	−5539.7	−4951.4
400	822.5	−5468.2	−5809.9	854.0	76.4	853.8	−5531.5	−4867.8
450	864.4	−5426.0	−5855.1	953.5	118.1	953.2	−5521.7	−4785.5
500	895.7	−5381.9	−5905.1	1046.2	161.4	1045.9	−5511.0	−4704.2
550	920.7	−5336.5	−5959.6	1132.8	205.8	1132.4	−5499.9	−4624.1
600	942.7	−5289.9	−6018.3	1213.9	250.9	1213.5	−5488.7	−4544.9
650	964.5	−5242.3	−6080.1	1290.2	296.7	1289.7	−5477.5	−4466.7
700	1001.4	−5193.4	−6147.2	1362.7	304.8	1362.3	−5466.2	−4389.4
732[b]	1046.5	−5160.6	−6191.6	1408.4	335.3	1407.9	−5458.2	−4340.4
750	961.0	−5143.1	−6217.1	1432.1	418.2	1431.5	−5454.8	−4312.9
800	943.3	−5095.6	−6290.3	1493.3	464.5	1492.7	−5447.8	−4237.0
850	938.4	−5048.6	−6366.4	1550.4	510.9	1549.8	−5443.5	−4161.5
900	935.7	−5001.8	−6445.3	1603.9	557.2	1603.3	−5440.4	−4086.2
950	933.9	−4955.0	−6526.7	1654.5	603.6	1653.9	−5439.7	−4010.9
1000	932.8	−4908.3	−6610.7	1702.3	650.0	1701.6	−5441.9	−3935.8

[a]Calculated values of C°_p.
[b]Transition point of $SrFe_{12}O_{19}$(s).

Table 6
Thermodynamic functions for the compound $SrFe_2O_4$(s)

T/K	$C_p{}^\circ$[a] ($J\,K^{-1}\,mol^{-1}$)	H° ($kJ\,mol^{-1}$)	G° ($kJ\,mol^{-1}$)	S° ($J\,K^{-1}\,mol^{-1}$)	$H_T{}^\circ - H_{298.15}{}^\circ$ ($kJ\,mol^{-1}$)	*fef* ($J\,K^{-1}\,mol^{-1}$)	$\Delta_f H^\circ$ ($kJ\,mol^{-1}$)	$\Delta_f G^\circ$ ($kJ\,mol^{-1}$)
Error	1.6%	±1.3	±1.2	±1.0	±0.6	±1.5	±1.4	±1.7
298.15	144.8	−1583.8	−1617.4	112.7	0	112.7	−1583.8	−1462.3
300	145.2	−1583.5	−1617.6	113.6	0.3	112.7	−1583.7	−1461.5
350	152.9	−1576.1	−1623.9	136.6	7.7	114.5	−1583.2	−1441.2
400	159.6	−1568.3	−1631.2	157.4	15.5	118.6	−1582.4	−1420.9
450	165.6	−1560.1	−1639.6	176.6	23.7	124.0	−1581.5	−1400.8
500	171.3	−1551.7	−1648.9	194.3	32.1	130.1	−1580.4	−1380.8
550	176.7	−1543.0	−1659.0	210.9	40.8	136.7	−1579.3	−1360.9
600	181.9	−1534.0	−1669.9	226.5	49.8	143.6	−1578.1	−1341.1
650	186.9	−1524.8	−1681.6	241.3	59.0	150.6	−1576.9	−1321.4
700	192.0	−1515.3	−1694.0	255.3	68.5	157.5	−1575.7	−1301.8
750	196.9	−1505.6	−1707.2	268.7	78.2	164.5	−1574.4	−1282.3
800	201.9	−1495.6	−1720.9	281.6	88.1	171.4	−1573.2	−1262.8
850	206.7	−1485.4	−1735.3	293.9	98.4	178.2	−1572.8	−1243.4
900	211.6	−1474.9	−1750.3	305.9	108.8	185.0	−1571.6	−1224.1
950	216.4	−1464.3	−1765.9	317.5	119.5	191.7	−1570.5	−1204.8
1000	221.2	−1453.3	−1782.0	328.7	130.5	198.2	−1569.7	−1185.6

[a]Calculated values of $C_p{}^\circ$.

$G^\circ(T)$, $\Delta_f H^\circ(T)$, $\Delta_f G^\circ(T)$ and free energy function (*fef*). The *fef* is defined as

$$fef = -\frac{\{G^\circ(T) - H^\circ(298.15)\}}{T}. \quad (26)$$

Isobaric molar heat capacities of ternary oxides of the system were extrapolated to 1000 K (Table 4) and standard molar Gibbs energy of formation for the compound $SrFe_{12}O_{19}$(s) from literature [13] and that of $SrFe_2O_4$(s), $Sr_2Fe_2O_5$(s) and $Sr_3Fe_2O_6$(s) were used as primary data for second law analysis. The molar heat capacity values of Sr(s), Fe(s) and O_2(g) required for the second law analysis have taken from the 'FactSage thermo-chemical database' [15]. In second law analysis of $SrFe_{12}O_{19}$(s), experimental heat capacity values were least square fitted in different temperature ranges as represented in Table 4 and the thermodynamic functions of $SrFe_{12}O_{19}$(s) were calculated using the 'FactSage' software. After calculation of all the thermodynamic functions, the values are tabulated at selected temperatures from 298 to 1000 K and represented

Table 7
Thermodynamic functions for the compound $Sr_2Fe_2O_5$(s)

T/K	C_p°[a] ($J\,K^{-1}\,mol^{-1}$)	H° ($kJ\,mol^{-1}$)	G° ($kJ\,mol^{-1}$)	S° ($J\,K^{-1}\,mol^{-1}$)	$H_T^\circ - H_{298.15}^\circ$ ($kJ\,mol^{-1}$)	*fef* ($J\,K^{-1}\,mol^{-1}$)	$\Delta_f H^\circ$ ($kJ\,mol^{-1}$)	$\Delta_f G^\circ$ ($kJ\,mol^{-1}$)
Error	1.6%	±1.6	±1.5	±1.2	±0.5	±1.8	±1.9	±3.0
298.15	186.3	−2142.7	−2202.3	199.8	0	199.8	−2142.7	−2000.0
300	186.7	−2142.4	−2202.6	200.9	0.3	199.7	−2142.6	−1999.1
350	195.9	−2132.8	−2213.4	230.4	9.9	202.1	−2142.1	−1975.2
400	203.6	−2122.8	−2225.6	257.1	19.9	207.3	−2141.2	−1951.4
450	210.5	−2112.4	−2239.1	281.5	30.3	214.3	−2140.2	−1927.7
500	216.8	−2101.8	−2253.8	304.0	40.9	222.1	−2139.1	−1904.2
550	222.8	−2090.8	−2269.5	324.9	51.9	230.5	−2137.9	−1880.7
600	228.6	−2079.5	−2286.2	344.6	63.2	239.2	−2136.7	−1857.4
650	234.2	−2067.9	−2303.9	363.1	74.8	248.0	−2135.5	−1834.2
700	239.7	−2056.1	−2322.5	380.7	86.6	256.9	−2134.2	−1811.1
750	245.1	−2043.9	−2341.9	397.4	98.8	265.7	−2132.9	−1788.0
800	250.4	−2031.6	−2362.3	413.4	111.1	274.5	−2131.7	−1765.1
850	255.7	−2018.9	−2383.3	428.7	123.8	283.1	−2132.1	−1742.1
900	260.9	−2005.9	−2405.1	443.5	136.7	291.6	−2130.8	−1719.2
950	266.1	−1992.8	−2427.6	457.7	149.9	299.9	−2129.7	−1696.4
1000	271.3	−1979.4	−2450.9	471.5	163.3	308.2	−2128.7	−1673.6

[a]Calculated values of C_p°.

Table 8
Thermodynamic functions for the compound $Sr_3Fe_2O_6$(s)

T/K	C_p°[a] ($J\,K^{-1}\,mol^{-1}$)	H° ($kJ\,mol^{-1}$)	G° ($kJ\,mol^{-1}$)	S° ($J\,K^{-1}\,mol^{-1}$)	$H_T^\circ - H_{298.15}^\circ$ ($kJ\,mol^{-1}$)	*fef* ($J\,K^{-1}\,mol^{-1}$)	$\Delta_f H^\circ$ ($kJ\,mol^{-1}$)	$\Delta_f G^\circ$ ($kJ\,mol^{-1}$)
Error	1.6%	±3.5	±2.8	±1.1	±0.5	±1.9	±5.2	±7.3
298.15	227.6	−2815.8	−2901.8	288.3	0	288.3	−2815.8	−2652.3
300	228.1	−2815.4	−2902.3	289.7	0.4	288.3	−2815.7	−2651.3
350	238.7	−2803.7	−2917.7	325.7	12.1	291.1	−2815.1	−2623.9
400	247.5	−2791.5	−2934.8	358.2	24.3	297.5	−2814.2	−2596.6
450	255.2	−2778.9	−2953.5	387.8	36.8	306.0	−2813.2	−2569.5
500	262.3	−2766.0	−2973.5	415.0	49.8	315.5	−2812.0	−2542.5
550	268.9	−2752.7	−2994.9	440.3	63.1	325.7	−2810.8	−2515.6
600	275.2	−2739.1	−3017.5	463.9	76.7	336.1	−2809.6	−2488.8
650	281.3	−2725.2	−3041.3	486.3	90.6	347.0	−2808.3	−2462.1
700	287.3	−2711.0	−3066.2	507.3	104.8	357.6	−2806.9	−2435.5
750	293.1	−2696.5	−3092.0	527.4	119.3	368.3	−2805.7	−2409.0
800	298.9	−2681.7	−3118.9	546.5	134.1	378.9	−2804.5	−2382.6
850	304.7	−2666.7	−3146.7	564.8	149.2	389.3	−2805.6	−2356.2
900	310.3	−2651.2	−3175.3	582.3	164.6	399.4	−2804.2	−2329.8
950	315.9	−2635.6	−3204.9	599.3	180.2	409.6	−2802.9	−2303.5
1000	321.5	−2619.6	−3235.3	615.6	196.2	419.4	−2801.9	−2277.2

[a]Calculated values of C_p°.

in Tables 5–8 for $SrFe_{12}O_{19}$(s), $SrFe_2O_4$(s), $Sr_2Fe_2O_5$(s) and $Sr_3Fe_2O_6$(s), respectively. The values of thermodynamic data generated in this study will enable the assessment of thermo-chemical stabilities of these ternary oxides of the system Sr–Fe–O in different chemical environments and it can be used for the optimization of oxygen potential and processing conditions required to prepare thin films of $SrFe_{12}O_{19}$(s) using different techniques.

Acknowledgments

The authors gratefully acknowledge the help of Dr. K. Krishnan and Dr. K.D. Singh Mudher for X-ray diffraction analysis.

References

[1] V. Berbenni, A. Marini, Mater. Res. Bull. 37 (2002) 221.
[2] A. Fossdal, M.-A. Einarsrud, T. Grande, J. Solid State Chem. 177 (2004) 2933.
[3] L.A. Garcia-Cerda, O.S. Rodriguez-Fernandez, P.J. resendiz-Hernandez, J. Alloys Compd. 369 (2004) 182.
[4] P. Tenaud, A. Morel, F. Kools, J.M. Le Breton, L. Lechevallier, J. Alloys Compd. 370 (2004) 331.
[5] J.F. Wang, C.B. Ponton, I.R. Harris, J. Magn. Magn. Mater. 234 (2001) 233.
[6] W.A. Kazamareck, B. Idikowski, K.H. Muller, J. Magn. Magn. Mater. 177–181 (1998) 921.
[7] Z.B. Guo, W.P. Ding, W. Zhong, J.R. Zang, Y.W. Do, J. Magn. Magn. Mater. 175 (1997) 333.
[8] A. Ataie, S. Heshmati-Manesh, J. Eur. Ceram. Soc. 21 (2001) 1951.
[9] H. Sato, T. Umeda, J. Mater. Trans. 34 (1993) 76.
[10] G. Elvin, I.P.P. Parkin, Q.T. Bui, L. Fernandez Barquin, Q.A. Pankhurst, A.V. Komarov, Y.G. Morozov, J. Mater. Sci. Lett. 16 (1997) 1237.
[11] M. Kakihana, J. Sol-Gel Sci. Tech. 6 (1996) 5.
[12] K. Shono, M. Gomi, M. Abe, Jpn. J. App. Phys. 21 (10) (1982) 1451.
[13] S.K. Rakshit, S.C. Parida, S. Dash, Z. Singh, R. Prasad, V. Venugopal, Mater. Res. Bull. 40 (2005) 323.
[14] M.W. Chase, Jr., JANAF Thermochemical Tables, 4th ed., J. Phys. Chem. Ref. Data, Monograph No. 9, 1995.
[15] FactSage, version 5.3.1, 1976–2004. Thermo-chemical database software, Thermfact, GTT Technologies, Germany.